Preferential concentration of particles in forced turbulent flows: Effects of gravity

Guodong Gai, Olivier Thomine, Abdellah Hadjadj, Sergey Kudriakov, Anthony Wachs

energies

MDPI

Article

Preferential Concentration of Particles in Forced Turbulent Flows: Effects of Gravity

Guodong Gai [1], Olivier Thomine [2], Abdellah Hadjadj [2,*], Sergey Kudriakov [3] and Anthony Wachs [1,4]

[1] Department of Mathematics, University of British Columbia, Vancouver, BC V6T 1Z2, Canada; guodong.gai@outlook.fr (G.G.)
[2] INSA, CORIA UMR-6614 CNRS, University of Normandy, 76000 Rouen, France; olivier.thomine@protonmail.com
[3] Service de Thermo-Hydraulique et de Mécanique des Fluides, CEA, Université Paris-Saclay, 91191 Gif-sur-Yvette, France
[4] Department of Chemical & Biological Engineering, University of British Columbia, Vancouver, BC V6T 1Z3, Canada
* Correspondence: abdellah.hadjadj@insa-rouen.fr

Abstract: The impact of gravity on the particle preferential concentration is investigated by direct numerical simulations in an Eulerian–Lagrangian framework for a large range of Stokes numbers $St_\eta = 0.01 \sim 4$. For particles with small Stokes numbers such as $St_\eta = 0.01$, the gravity has minor effects on the particle spatial distribution in the turbulence. With increasing St_η, stripped structures of the high number density of particles appear and expand along the gravity direction. Different evaluation methods of particle preferential concentration are discussed such as the spatial distribution, the box index, and the probability density function. The number density of particles in the accumulating regions reduced under the influence of gravity. The reduction becomes prominent for the particle cloud at Stokes number $St_\eta \approx 1$, especially in the clusters of high particle number density. For large Stokes number St_η, the slip velocity significantly increases due to the particle gravity. Due to the gravity, the particle concentration reduces globally, particularly in the low vorticity regions. For the Stokes number range explored in this paper, gravity has a considerable impact on the particle-turbulence interaction.

Keywords: gravity effect; incompressible flow; particle-turbulence interaction; preferential concentration; stokes number

Citation: Gai, G.; Thomine, O.; Hadjadj, A.; Kudriakov, S.; Wachs, A. Preferential Concentration of Particles in Forced Turbulent Flows: Effects of Gravity. *Energies* **2023**, *16*, 2910. https://doi.org/10.3390/en16062910

Academic Editor: Bjørn H. Hjertager

Received: 23 January 2023
Revised: 25 February 2023
Accepted: 17 March 2023
Published: 22 March 2023

1. Introduction

Particle-laden turbulent flows are ubiquitous in the environment and are widely employed in a variety of industrial applications, including particle air pollution, river sedimentation, ocean dynamics, liquid fuel in engines and fire-mitigation spray systems [1–4]. Turbulence impacts the fundamental ecology of the ocean by affecting the spatial distribution of aquatic microorganisms [5]. Turbulence in the airflow and particle segregation are responsible for atmospheric particle pollution, which is a great threat to human health on a worldwide scale [6]. Spray evaporation and mixing are crucial inside the combustion chamber of engines, which is closely related to the droplet-turbulence interaction. For decades, the interactions between the dispersed particles and the carrier phase have been widely studied [7,8]. Small particles act as tracers in turbulent flow in a highly dilute system, but in a dense two-phase system, the particles can reversely influence the carrier phase flow [9].

The accumulation of particles in specific regions of the turbulence field is referred to as preferential concentration, which is due to the centrifuging of particles away from vortex cores in the dilute particle-laden flow. It has substantial implications for droplet combustion, turbulence modulation, and other relevant applications. Many studies using

one-way formalism, in which the effects of the particles on the carrier phase are neglected, demonstrate the importance of Stokes number St_η on the preferential concentration of the particles [10,11]. Using time scale of Kolmogorov τ_κ, the preferential concentration of particles reaches a peak at the Stokes number $St_\eta \approx 1$ [12]. The heavier-than-fluid particles have the tendency to accumulate to form clusters in regions of low vorticity (high strain) in a turbulent fluid flow. However, the lighter-than-fluid particles tend to form clusters in high vorticity regions [13].

In the case of two-way coupling, in which the particles have a reverse influence on the carrier phase, the Stokes number and mass loading are known to be dominant parameters of the modulation of homogeneous isotropic turbulence (HIT) [13]. At large wavenumbers of the energy spectrum, the energy increases with the presence of particles with an increase in the dissipation, as indicated in the studies of a stationary HIT [9,14]. Several aspects have been investigated to explain the complicated physical mechanisms of particle-laden HIT such as phase-coupling function, energy spectra and length/time scales [15]. The phenomena such as inertia effects, crossing-trajectories, and continuity effects need to be considered. The ratio of particle response time and the Kolmogorov time scale τ_p/τ_κ is proposed to categorize the enhancement and mitigation of the turbulence intensity [16]. More sophisticated four-way coupling between the particles and the carrier phase are investigated for dense particle-laden flows ($\tau_v > 10^{-3}$) [17]. Stokes number St_η and volume fraction τ_v are taken as key parameters to analyze the particle preferential concentration and turbulence modulation. According to the coupling spectrum, the particles transfer energy from the large to the small turbulence scales [15]. Regardless of the coupling method applied, the preferential concentration of particles is of vital importance for the study of fluid-particle interactions.

Albeit the fact that many numerical researches have concentrated on the gravityless flow configuration, the interest in the effect of gravitation on particle dispersion dates back to early times and still remains an active field of research [18,19]. The gravity is reported to be consistent with crossing trajectories, reducing unequally the particle diffusion coefficients [20]. The effects of gravity and homogeneous shear on the dispersion of heavy particles were addressed in the work of [21], using direct numerical simulation of low Reynolds number in both decaying and forced isotropic turbulence. The particle dispersion was observed to be greatly reduced by externally imposed gravity. Elghobashi et al. investigated the main physical mechanisms responsible for the modification of isotropic turbulence by dispersed solid particles and highlighted the contribution of particle gravity on the turbulence modulation [16]. The gravity influence on collisions of mono-dispersed droplets in HIT was investigated in the work of [22]. In certain Stokes and Reynolds regimes, the collision frequencies are found to be significantly reduced, mainly owing to the decrease in the droplet relative velocity with the presence of gravity. Recent experiments report that both inertia and gravity are key ingredients to understand the dynamics and transport of heavy particles in forced homogeneous turbulence. Clustering is confirmed to be most intense for $St_\eta \approx 1$ with consideration of particle gravity, but it extends over larger scales for heavier particles [23,24]. The gravity is reported to decrease particle clustering at low Stokes number and increase clustering at high Stokes numbers [25]. The preferential concentration of particles in high-strain/low-vorticity regions is measured, but its impact on the global statistics is reported to be moderate [26]. Furthermore, the effects of gravity can be significant in other types of two-phase systems such as bubble flows [27], and for other physical phenomena such as polydisperse particle preferential concentration [28].

The objective of this research is to investigate quantitatively and bring new insights to the impact of gravity on the preferential concentration of particles at various Stokes numbers, as well as its influence on particle slip velocities. In Section 2, the governing equations and preliminary assumptions for the carrier and dispersed phases are introduced; Section 3 presents the numerical configuration of the simulations; Section 4 shows the simulation results on the particle preferential concentration with the presence of gravity

using different quantification tools; the effects of gravity on the slip velocity are discussed in Section 5; a comprehensive summary of the current study is followed in Section 6.

2. Numerical Method

A two-phase system containing a particle cloud inside a gaseous carrier phase with initial turbulence is investigated using direct numerical simulations. A spectral solver with forced homogeneous isotropic turbulence, implemented in the in-house code Asphodele, developed in CORIA Rouen, is employed in the Eulerian–Lagrangian framework [28].

2.1. Carrier Phase

The three-dimensional simulations in this study are based on a 3D forced Homogeneous Isotropic Turbulence (HIT) for the gas phase resolved in a cubic domain with periodic boundary conditions. Navier-Stokes equations for an incompressible fluid with a constant viscosity are solved in the spectral domain. The forcing scheme is based on an initial solution for a HIT obtained based on a model for the energy spectrum, which has the following expression [29,30]:

$$E_m(\kappa) = 1.5 < \varepsilon >^{2/3} \kappa^{-5/3} f_L(\kappa L) f_\eta(\kappa\eta) \tag{1}$$

where:

$$f_L(\kappa L) = \left(\frac{\kappa L}{[(\kappa L)^2 + c_L]^{1/2}} \right)^{17/3} \tag{2}$$

$$f_\eta(\eta L) = \exp\left(-5.2 \left[((\kappa\eta)^4 + c_\eta^4)^{1/4} - c_\eta \right] \right) \tag{3}$$

where ν denotes the fluid viscosity, $< \varepsilon >$ is the current mean dissipation over the whole spectral domain, L characterizes the size of the large eddies, and f_L and f_η are two non-dimensional functions which denote the shape of the energy containing range and the shape of the dissipation range. f_L tends to one with large κL whereas f_η approaches 1 with small $\kappa\eta$. The constants c_L and c_η are determined in a way that the integration of $E_m(\kappa)$ and $2\nu k^2 E_m(\kappa)$ gives the turbulent kinetic energy k and the dissipation ε, respectively [31].

As an extension of [31], a fully controlled deterministic turbulence forcing scheme was proposed by [30], in order to get a statistically stationary spectral turbulence. A "negative" energy is added to the simulated spectrum, to determine the spectral gas velocity, using the following equation [30]:

$$\frac{\partial \hat{u}}{\partial t} = \hat{a} + \frac{f_\kappa}{\tau_\kappa} \hat{u} \text{ with, } \tau_\kappa = \frac{1}{2} \sqrt{\frac{\nu}{< \varepsilon >}} \tag{4}$$

where $\hat{a}$ is the Navier-Stokes contribution of the incompressible flow; f_κ is the time-dependent forcing function which varies with the wave number magnitude κ and τ_κ denotes the Kolmogorov time scale. The time evolution of the studied energy spectrum E_s can be written as [30]:

$$\frac{dE_s}{dt} = C_\kappa + 2\frac{f_\kappa}{\tau_\kappa} E_s \text{ with, } f_\kappa = \frac{F_\kappa}{2E_s(\kappa, t)} \left(\alpha_f(t) E_m(t) - E_s(\kappa, t) \right) \tag{5}$$

where C_κ denotes the energy contribution without any source term. The objective of the model is to relax the simulated spectrum E_s towards a model spectrum E_m for a specific range of low wave numbers. F_κ is a filter function and α_f is a coefficient which controls the evolution of the mean turbulent energy $< k >$. The Reynolds number of the turbulence is fixed to be $Re_t = 1000$ and the Taylor-Reynolds number is $Re_\lambda = 122.5$ and the Froude number is $F_r = 1.0$. $\tau_\eta = 0.02\ s$ denotes the Kolmogorov time scale. More details about the implementation and validations the spectral DNS solver can be found in the work of [28,32,33].

2.2. Dispersed Phase

The particles are taken to be smaller than the Kolmogorov length scale (η) of the gas turbulence and a point-mass particle is assumed in the simulations [34]. The drag force on the particle is calculated as a function of the difference of gas flow velocity $\mathbf{u}(\mathbf{x}, t)$ and particle velocity $\mathbf{V}(t)$. For a particle located at $\mathbf{x}$, the general motion equation gives [35]:

$$m_p \frac{d\mathbf{V}(t)}{dt} = \mathbf{F_d} + m_p \boldsymbol{g}, \tag{6}$$

with:

$$\mathbf{F_d} = \frac{\pi}{8} \rho_p D^2 C_d |\mathbf{u}(\mathbf{x}, t) - \mathbf{V}(t)| (\mathbf{u}(\mathbf{x}, t) - \mathbf{V}(t)), \tag{7}$$

where $m_p = \pi \rho_p D^3/6$ is the particle mass and ρ_p is the particle density. The total force exerted on the particle contains the gravity ($\boldsymbol{g} = 9.8$ m/s^2) and the drag force $\mathbf{F_d}$ and C_d is the drag coefficient:

$$C_d = \frac{24}{Re_p} \left(1 + 0.15 Re_p^{0.687}\right), \tag{8}$$

with:

$$Re_p = \frac{\rho_g |\mathbf{u}(\mathbf{x}, t) - \mathbf{V}(t)| D}{\mu_g}. \tag{9}$$

Re_p is the particular Reynolds number related to the flow around the particle and μ_g is the dynamic viscosity of the gas. The non-linear drag model is used in this study because with the increase of the Stokes number, the particle Reynolds number Re_p can be up to 50.

The followings are the assumptions and simplifications used in the current work's numerical simulations: (i) the gas obeys a perfect-gas law and only the viscous drag forces and gravity are considered to act on the particles; (ii) the particles are considered as spherical, inert, rigid and of uniform diameter ($D < \eta$); (iii) the volume fraction of the particles is small ($\tau_v < 10^{-3}$) so that the collision between particles can be neglected; (iv) The particle-to-gas density ratio is taken to be $\rho_p/\rho_g = 553$, the Basset force can be neglected [7] and we assume that the particles do not spin so that the Magnus force is neglected; (v) The change in the topology of the particle cloud is deemed to be influenced by both drag and particle gravity.

3. Numerical Configuration

We consider a cubic box of length $L_x = L_y = L_z$, which contains a turbulent gaseous phase that reaches a statistically steady state. The characteristic values of the gas turbulence and the reference parameters can be found in [32]. With a zero-initial velocity, monodisperse no-evaporating particles are initially seeded randomly in the box. The particle motion is affected by the drag force and the gravity is assigned along the z-axis direction. With fixed turbulent properties, the simulations are carried out by imposing values to the particle response time parameter τ_p. Then the Stokes number $St_\eta = \tau_p/\tau_\kappa$ can be obtained using the Kolmogorov time scale τ_κ. In this 3D configuration, a grid mesh of 128^3 is used. The Eulerian–Lagrangian approach is used for the fluid with a point mass approach for the particle. Periodical boundary conditions are set along the three axis.

The Courant-Friedrich-Levy condition is satisfied to guarantee the numerical stability of the advection term in the momentum conservation equation. We choose the time step to satisfy that $CFL < 0.8$.

4. Effects of Gravity on Preferential Concentration

In this section, a series of direct numerical simulations (DNS) are performed for different Stokes numbers $0.01 < St_\eta < 4.0$. Since the particle diameter and the particle volume fraction are small, we consider a one-way formalism in the current study. The particle are directly affected by the drag force and the gravity. We measure their settling velocities after a simulation time of $t/\tau_\kappa = 27$.

4.1. Spatial Distribution of Particles

Figure 1 depicts the particle number density on the plane $y = 0.5L_y$ for different Stokes numbers $St_\eta = 0.01, 1.0$ and 2.0 at $t/\tau_\kappa = 27$. Results of simulations with and without gravity exerted on the particles are provided for comparison. The particle preferential concentration is noted to be most significant for $St_\eta \approx 1$ for the case without gravity. Effects of gravity are not evident for small Stokes number cases, such as $St_\eta < 0.1$ in Figure 1a,d. For $St_\eta > 0.5$, one can see the particle preferential concentration becomes important in the regions of low-vorticity (high strain) due to the inertia. The impact of gravity on the particle preferential concentration can be noticed for $St_\eta > 0.5$. The highest density of the particle clusters is slightly affected by the consideration of gravity by comparing Figure 1b,e. In general, the particle density can be reduced by the presence of gravity. Instead of accumulating in the low-vorticity region, the clustering pattern becomes striped for higher Stokes numbers, similar to the result in [36]. In comparison to inertia, gravity has a greater impact when $St_\eta > 1.0$, as attested by the strong clustering pattern shown in Figure 1e,f. For a higher Stokes number $St_\eta > 2.0$, the particle preferential concentration becomes less noticeable, since the gravity is much more important than the inertia of the particles.

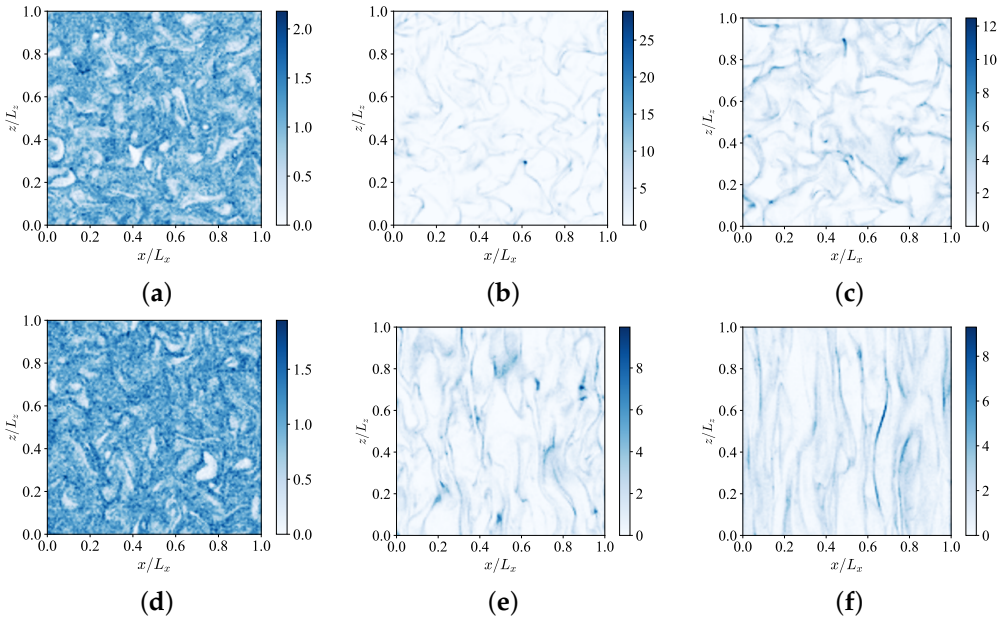

Figure 1. Effects of gravity on preferential concentration: $y = 0.5L_y$ plane; N: without gravity, G: $g = 9.8$ m/s^2. (**a**) $St_\eta = 0.01$, N; (**b**) $St_\eta = 1.0$, N; (**c**) $St_\eta = 2.0$, N; (**d**) $St_\eta = 0.01$, G; (**e**) $St_\eta = 1.0$, G; (**f**) $St_\eta = 2.0$, G.

Figure 2 presents the particle preferential concentration with and without gravity for different Stokes numbers St_η on the plane $x - y$ (perpendicular to the z axis). Similar to the particle distribution on the $x - z$ plane, the gravity has a negligible effect on the clustering for a small Stokes number, as depicted in Figure 2a,d. The consideration of particle gravity can reduce the maximum particle concentration for higher Stokes numbers. However, the pattern of preferential concentration remains similar to the case without gravity on the $x - y$ plane, as shown in Figure 2e,f. In comparison to the gravityless case, the clustering structures can be more compact. Overall, the clustering pattern becomes significantly less isotropic when considering gravity, especially when the Stokes number exceeds 1.

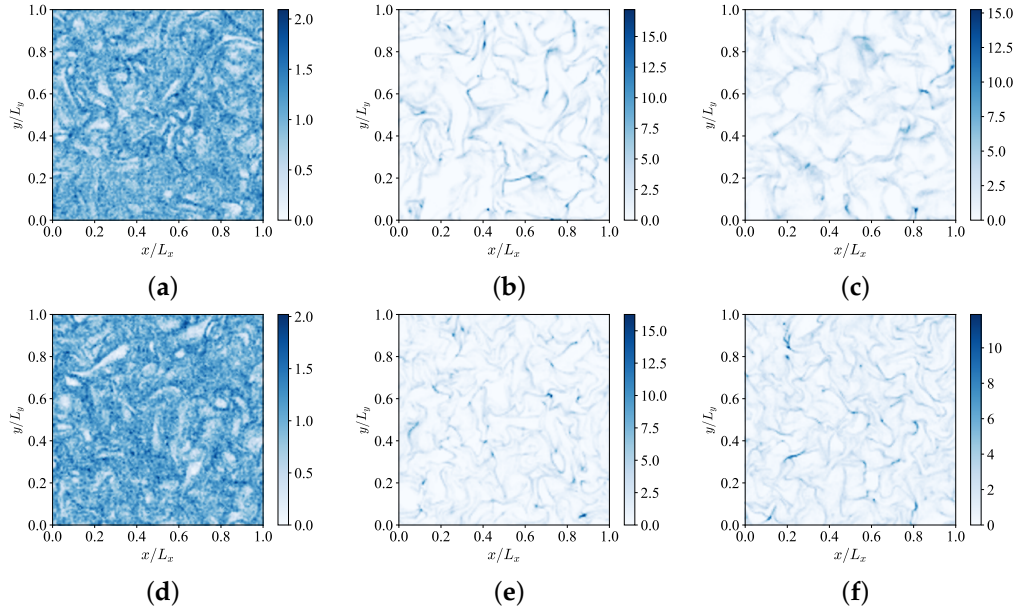

Figure 2. Effects of gravity on preferential concentration: $z = 0.5L_z$ plane; N: without gravity, G: $g = 9.8$ m/s^2. (**a**) $St_\eta = 0.01$, N; (**b**) $St_\eta = 1.0$, N; (**c**) $St_\eta = 2.0$, N; (**d**) $St_\eta = 0.01$, G; (**e**) $St_\eta = 1.0$, G; (**f**) $St_\eta = 2.0$, G.

4.2. Particle Preferential Concentration and Vorticity

Let N/N_0 denote the volumic particle number density normalized by its initial value at the beginning of the simulation. Figure 3 shows the correlation between the normalized particle number density and the gas phase vorticity magnitude, where $\overline{\omega}$ denotes the mean vorticity magnitude for the gas turbulence.

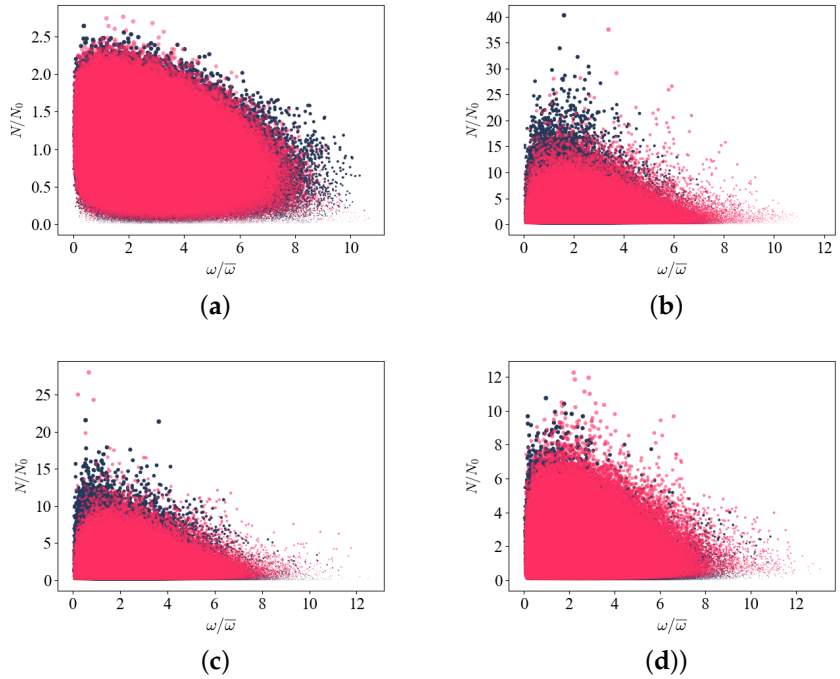

Figure 3. Evolution of particle number N/N_0 density as a function of normalized vorticity magnitude $\omega/\overline{\omega}$ for different Stokes number; blue dots: without gravity, red dots: with gravity. (**a**) $St_\eta = 0.01$; (**b**) $St_\eta = 1.00$; (**c**) $St_\eta = 2.00$; (**d**) $St_\eta = 4.00$.

From Figure 3a, we can see that the high values of the particle number density only exist in the region of low vorticity in both the cases with and without gravity for $St_\eta = 0.01$ [37]. An evident decrease of the particle number density can be noted, when we consider the effect of gravity on the system of Stokes number $St_\eta = 1.0$, notably in the low-vorticity zone. From Figure 3b,c the effects of gravity are more conspicuous in these regions. For higher St_η, this reduction of particle density still exists but with a lower magnitude.

For $St_\eta = 4.0$, the effects of particle gravity become a bit blurred as depicted in Figure 3d. One can infer that the particle clustering becomes no more affected by particle gravity for $St_\eta > 4.0$. The largest deviation of the particle number density is perceived around $St_\eta = 1.0$.

4.3. Box-Counting Measurement

Apart from the qualitative analysis of the preferential concentration, we also investigate the particle preferential concentration quantitatively. In addition to the specific spatial distribution of the particles in turbulence, the global behavior of the segregation is also an important aspect of the particle turbulence interaction. In the following, the Lagrangian particles are projected and counted in each computational cell (cube with the size of the grid step) of the simulation domain. The effects of particle gravity are investigated in two different ways: using the maximal particle number density and the box index (BI).

Figure 4 shows the global effects of gravity on the particle clustering. The maximal particle number density is firstly considered. Figure 4a shows that gravity almost has no effects on the maximal particle number density for small Stokes numbers $St_\eta < 0.5$ and large Stokes numbers $St_\eta > 2.0$. At intermediate Stokes numbers $0.5 < St_\eta < 2.0$, gravity decreases the maximum particle number density. This decrease is also noticeable in the Figures 1 and 2. Since the maximal value of particle concentration evolves in time, this parameter for preferential concentration is indicative at best but not reliable enough to characterize our systems.

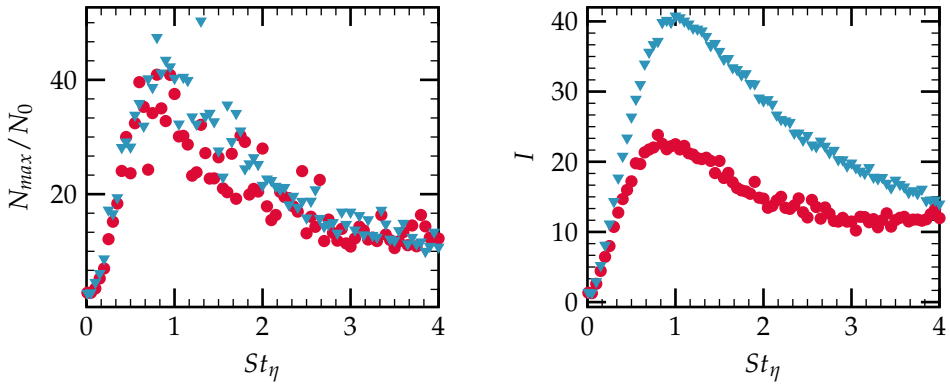

Figure 4. Gravity effects on global preferential concentration of particles in turbulence for varying St_η at $t/\tau_\kappa = 27$; (**a**) maximal particle number density, (**b**) box index I; simulations without gravity in blue triangle points (▼), with gravity in red spherical points (●).

The global preferential concentration of particles in turbulence can be measured by the box index (BI). Even though the box index is not sensitive to the shape of particle clusters, it is convenient to use and can clearly characterize the particle preferential concentration. One expression of the BI is the normalized variance of the particle number density [38,39]:

$$I(N_p, N_b) = \frac{\frac{1}{N_b}\Sigma_{b\in B}\left(N_{p,b} - N^0_{p,b}\right)^2}{\left(\frac{1}{N_b}\Sigma_{b\in B}N_{p,b}\right)^2} = \frac{N_b}{N_p^2}\Sigma_{b\in B}\left(N_{p,b} - N^0_{p,b}\right)^2 \quad (10)$$

where N_p is the total number of the particles in the domain; $N_{p,b}$ is the number of particles in the cubic box b (the cube box of edge length of Δx); $N^0_{p,b}$ represents the initial number of particles per box; B is the set of these boxes and N_b is the number density of particles. The box index I is a reliable marker of particle preferential concentration for large quantities of particles in the domain N_p, which is true in our case.

The box index I is calculated for simulations with different Stokes numbers and presented in Figure 4b. From Equation (10) we know that a higher value of I indicates stronger particle clustering in the two-phase system. A discernible reduction of I is noted for the cases with gravity, supporting the findings discussed in the above sections. For the range of Stokes number studied $0.01 < St_\eta < 4.0$, particle gravity's influence on the particle preferential concentration is the strongest for systems of $St_\eta \approx 1.0$, with a I reduction of 45% compared to the gravityless case. The maximal box index I moves slightly to the small particles, compared to the gravityless case. The influence decays gradually as St_η increases or decreases from 1. For $St_\eta = 0.01$ and $St_\eta = 4.0$, we cannot observe distinguishable effects.

4.4. Particle Number Density

Another useful tool to quantify the preferential concentration is the probability density function (PDF) of particle number density based on the box-counting method [38,40].

Figure 5 shows the PDF of normalized particle number density for different Stokes numbers $0.01 < St_\eta < 4.0$. Again, we note that particle gravity has minor effects on the system for Stokes numbers much larger or lower than $St_\eta = 1.0$, as depicted in Figure 5a,d. When the Stokes number gets close to 1, the consideration of particle gravity leads to a weaker particle preferential concentration, which is can be plainly seen from Figure 5b,c. These observations are consistent with our previous discussions. More precisely, from Figure 5, the impact of gravity on preferential concentration is more important to particle clusters of high number densities, which cannot be clearly shown using maximal particle number density N_{max}/N_0 in Figure 4a. In order to elucidate more clearly the mechanisms of the particle preferential concentration, various measurement methods are needed.

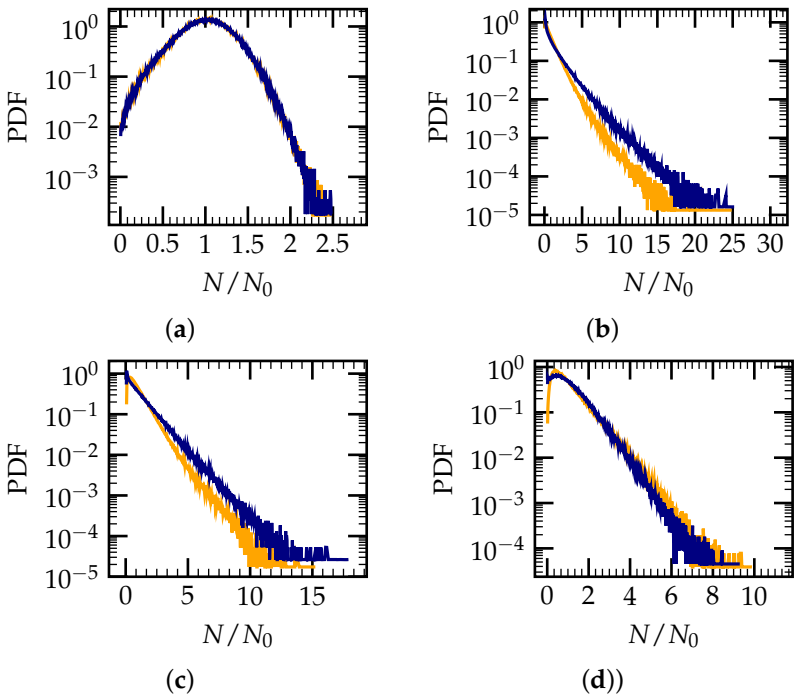

Figure 5. PDF of normalized particle number density N/N_0 for different Stokes numbers at $t/\tau_\kappa = 27$; orange line: with gravity (——) and blue line: without gravity (——). (**a**) $St_\eta = 0.01$; (**b**) $St_\eta = 1.00$; (**c**) $St_\eta = 2.00$; (**d**) $St_\eta = 4.00$.

5. Effects of Gravity on Slip Velocity

Particle gravity not only alters the preferential concentration, it also affects the dynamic properties of particle clusters directly. In this section, the evolution of particle slip velocity is investigated numerically.

The particle slip velocity is crucial for the evaluation of particle turbulence interactions [41]. Figure 6 shows the evolution of the particle slip velocity PDF for different Stokes numbers, where the particle slip velocity is non-dimensionalized by the RMS velocity of the carrier phase. The particle slip velocity $v_{s,i}$ and the mean velocity of the carrier phase U_0 are defined by:

$$v_{s,i} = \sqrt{\sum_{j=1}^{3} (\boldsymbol{V}_{i,j} - \boldsymbol{u}_{i,j})^2} \quad \text{and} \quad U_0 = \sqrt{\sum_{j=1}^{3} \overline{u_j}^2} \tag{11}$$

where $\boldsymbol{V}_{i,j}$ and $\boldsymbol{u}_{i,j}$ denote the jth component of the particle and fluid velocity in cell i, respectively. $\overline{u_j}$ is the jth component of average gas velocity.

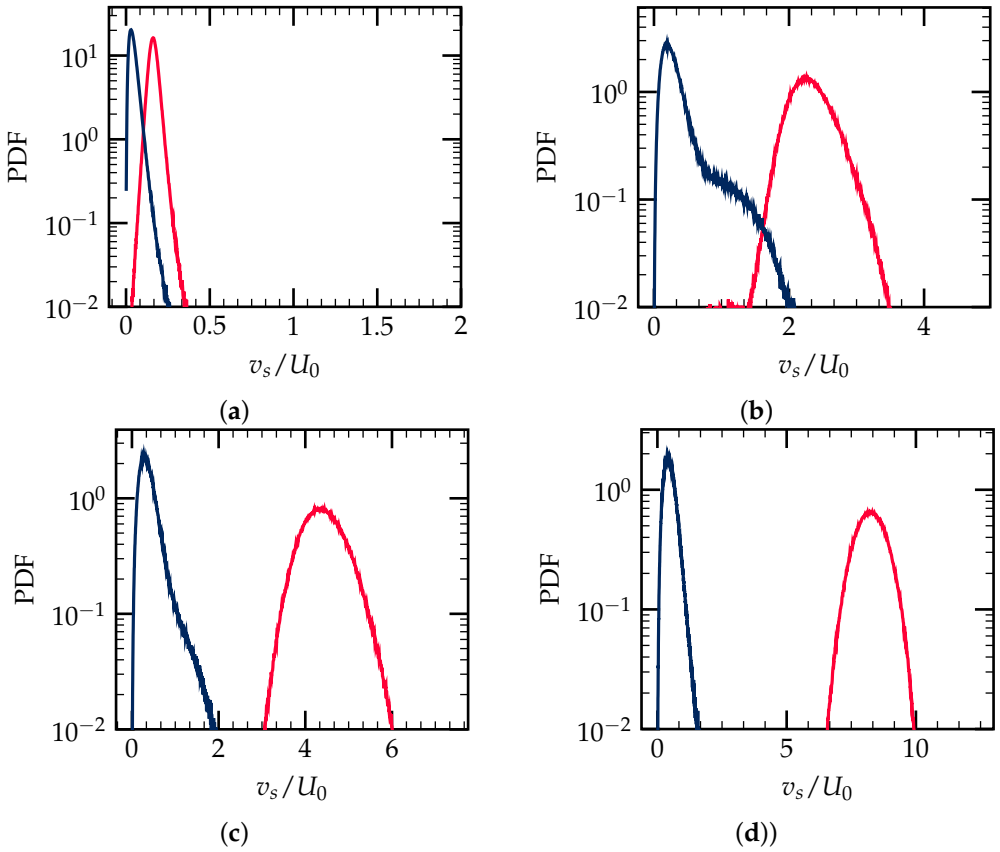

Figure 6. Evolution of normalized particle slip velocity PDF for different initial Stokes numbers at $t/\tau_\kappa = 27$; red curve: with gravity (——), blue curve: without gravity (——); v_s/U_0 the normalized particle slip velocity. (**a**) $St_\eta = 0.01$; (**b**) $St_\eta = 1.00$; (**c**) $St_\eta = 2.00$; (**d**) $St_\eta = 4.00$.

For the simulations without gravity, we note that the slip velocity increases with Stokes numbers. When $St_\eta > 1$, the PDF seems to change very slightly with increasing Stokes number, as shown in Figure 6b–d. The maximum slip velocity v_s/U_0 ranges from 1.5 to 3.0, while with gravity, the maximal slip velocity can increase to $v_s/U_0 = 10$. This is due to the fact that the particles become less sensitive to the motion of the surrounding gas with increasing St_η. Without gravity, the lag between particle and gas velocity increases with St_η.

When particle gravity is taken into account, the magnitude of slip velocity rises with Stokes number St_η as a result of high settling velocity. Different from the aforementioned

discussions on particle clustering, even for very small Stokes number $St_\eta = 0.01$, the average slip velocity is increased by gravity, in comparison to the gravityless case, as presented in Figure 6a. For higher Stokes numbers, we observe that the two curves separate gradually. The span of slip velocity distribution gets wider at a higher St_η.

To summarize, particle gravity has non-negligible effects on the slip velocity evolution for the range of Stokes number investigated in the current study. We would like to remind the reader that that only *one-way* formalism is used in our simulations, and therefore we expect the slip velocity properties to behave differently for larger particles (with higher St_η) for which *two-way* interactions may become indispensable to be introduced in the numerical model.

Figure 7a gives the setting velocity PDF for different Stokes numbers St_η. Apparently, with an increasing St_η, the settling velocity spans a narrower range of values and the magnitude of its mean value increases. We plot in Figure 7b the settling velocity in cases with gravity and the analytical settling velocity without any gas turbulence (i.e., in an otherwise quiescent fluid) as a function of St_η. A clear reduction of the settling velocity can be observed due to the gravity in the forced particle-laden turbulent flow.

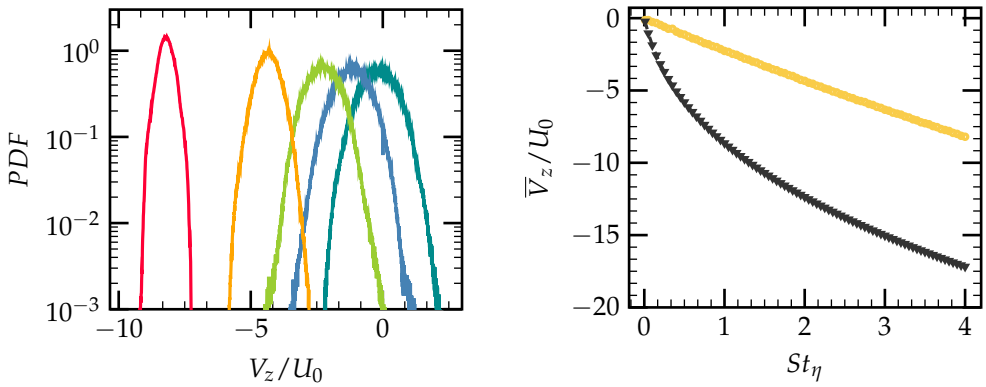

(**a**) (**b**)

Figure 7. (**a**) Settling velocity PDF: $St_\eta = 0.01$ (—), $St_\eta = 0.05$ (—), $St_\eta = 1.0$ (—), $St_\eta = 2.0$ (—), $St_\eta = 4.0$ (—); and (**b**) comparison between analytical and numerical simulation results with consideration of particle gravity: turbulence forced (○), free fall (—▼—). (**a**) Settling velocity PDF; (**b**) Forced turbulence (DNS) v.s. free fall.

6. Conclusions

The preferential concentration of particles in forced homogeneous isotropic turbulence has been investigated quantitatively using direct numerical simulations with consideration of particle gravity.

With the presence of an externally imposed body force, the global number density of particles in the gas phase forced turbulence is significantly reduced especially for Stokes number $St_\eta \approx 1$. Along the gravity direction, particle clusters form stripped structures at large Stokes numbers. When compared to the case without gravity, the box-counting measurement indicates a maximum reduction of roughly 45% of the box index, which occurs for the Stokes number $St_\eta \approx 1$. The maximum box index shifts to the smaller particles, with St_η slightly less than 1, compared to the gravityless case. The impact of gravity on particle concentration is noted to be important for clusters of high number densities. Overall, the consideration of particle gravity can change significantly the preferential concentration as well as the particle dispersion structures in the homogeneous isotropic turbulence. For the range of Stokes numbers considered in the current study, the slip velocity is effectively accelerated by the presence of particle gravity. Compared to the free-falling particle's analytical settling velocity in still fluid, the carrier phase turbulence efficiently reduces the particle settling velocity.

Gravity has a significant impact on particle preferential concentration over the Stokes number range studied. It should be considered while performing high-fidelity numerical simulations of particle-laden turbulent flow. Understanding the preferential concentration in the microscale using DNS simulation is beneficial for the meso- and macro-scale industrial applications. In droplet combustion and turbulent particle air pollution, the turbulence modification by particles is significant. As a follow up of the one-way coupling simulations carried out in this study, it would be valuable to perform two-way coupling numerical simulations in the future to obtain more insights into the effects of particle gravity, in particular at larger Stokes numbers. In addition, our future work is to perform particle-resolved DNS and get a more accurate and insightful understanding of the flow of particle interactions.

Author Contributions: Investigation, Validation, Visualization, Writing—original draft, G.G.; Conceptualization, Data curation, Software, O.T.; Methodology, Funding acquisition, Resources, Supervision, Writing—review & editing, A.H.; Conceptualization, Methodology S.K.; Writing—review & editing, A.W. All authors discussed the results and contributed to the final manuscript.

Funding: G. Gai would like to thank the Pacific Institute of Mathematical Sciences for their support through his PIMS-CNRS post-doctoral fellowship.

Institutional Review Board Statement: Not applicable

Informed Consent Statement: Not applicable

Data Availability Statement: The data supporting the findings of this study are available upon request from the authors.

Conflicts of Interest: The authors declare no conflict of interest.

Symbols and Abbreviations

The following symbols and abbreviations are used in this manuscript:

C_d	Drag coefficient
E_m	Energy spectrum
Fr	Froude number
Re_p	Particle Reynolds number
Re_t	Turbulent Reynolds number
Re_λ	Taylor Reynolds number
St_η	Stokes number
D	Particle diameter
I	Box index
L	Characteristic size of large eddies
L_i	Computational domain size in direction i
N	Particle number density
U_0	Mean velocity of the gas
V_z	Particle settling velocity
k	Turbulent kinetic energy
μ_g	Dynamic viscosity of gas
m_p	Particle mass
v_s	Slip velocity
$\mathbf{u}$	Gas flow velocity
$\mathbf{g}$	Gravity
$\mathbf{V}$	Particle velocity
$\mathbf{F}_d$	Drag force
ε	Turbulent dissipation rate
η	Kolmogorov length scale
κ	wave number magnitude
ν	Fluid viscosity
ρ_g	Gas density
ρ_p	Particle density

τ_p	Particle relaxation time
τ_v	Particle volume fraction
τ_κ	Kolmogorov time scale
ω	Vorticity of gas flow
$\overline{\omega}$	Mean vorticity magnitude
BI	Box index
HIT	Homogeneous isotropic turbulence
PDF	Probability density function
RMS	Root mean square

References

1. Williams, R.; Follows, M. *Ocean Dynamics and the Carbon Cycle: Principles and Mechanisms*; Cambridge University Press: Cambridge, UK, 2011. [CrossRef]
2. Javid, K.; Ali, N.; Asghar, Z. Rheological and magnetic effects on a fluid flow in a curved channel with different peristaltic wave profiles. *J. Braz. Soc. Mech. Sci.* **2019**, *41*, 483. [CrossRef]
3. Gai, G.; Kudriakov, S.; Rogg, B.; Hadjadj, A.; Studer, E.; Thomine, O. Numerical study on laminar flame velocity of hydrogen-air combustion under water spray effects. *Int. J. Hydrog. Energy* **2019**, *44*, 17015–17029. . [CrossRef]
4. Asghar, Z.; Javid, K.; Waqas, M.; Ghaffari, A.; Khan, W.A. Cilia-driven fluid flow in a curved channel: Effects of complex wave and porous medium. *Fluid Dyn. Res.* **2020**, *52*, 015514. [CrossRef]
5. Borgnino, M.; Arrieta, J.; Boffetta, G.; Lillo, F.D.; Tuval, I. Turbulence induces clustering and segregation of non-motile, buoyancy-regulating phytoplankton. *J. R. Soc. Interface* **2019**, *16*, 20190324. [CrossRef] [PubMed]
6. Li, D.; Luo, K.; Fan, J. Modulation of turbulence by dispersed solid particles in a spatially developing flat-plate boundary layer. *J. Fluid Mech.* **2016**, *802*, 359–394. [CrossRef]
7. Thomine, O. Development of Multi-Scale Methods for the Numerical Simulation of Diphasic Reactive Flows. Ph.D. Thesis, University of Rouen, Rouen, France, 2011.
8. Thomine, O.; Gai, G.; Hadjadj, A.; Kudriakov, S. Phenomenology of a two-phase laminar flame interacting with a heated cylinder. *Int. J. Heat Mass Transf.* **2021**, *168*, 120867. . [CrossRef]
9. Squires, K.; Eaton, J. Particle response and turbulence modification in isotropic turbulence. *Phys. Fluids A Fluid Dyn.* **1990**, *2*, 1191–1203. [CrossRef]
10. Eaton, J.; Fessler, J. Particle response and turbulence modification in isotropic turbulence. *Int. J. Multiph. Flow.* **1994**, *20*, 169–209. [CrossRef]
11. Sigurgeirsson, H.; Stuart, A. A model for preferential concentration. *Phys. Fluids* **2002**, *14*, 4352–4361. . [CrossRef]
12. Wang, L.P.; Maxey, M. Settling velocity and concentration distribution of heavy particles in homogeneous isotropic turbulence. *J. Fluid Mech.* **1993**, *256*, 27–68. [CrossRef]
13. Balachandar, S.; Eaton, J. Turbulent Dispersed Multiphase Flow. *Annu. Rev. Fluid Mech.* **2010**, *42*, 111–133. [CrossRef]
14. Sundaram, S.; Collins, L. A numerical study of the modulation of isotropic turbulence by suspended particles. *J. Fluid Mech.* **1999**, *379*, 105–143. [CrossRef]
15. Mallouppas, G.; George, W.; van Wachem, B. Dissipation and inter-scale transfer in fully coupled particle and fluid motions in homogeneous isotropic forced turbulence. *Int. J. Heat Fluid Flow* **2017**, *67*, 74–85. . [CrossRef]
16. Ferrante, A.; Elghobashi, S. On the physical mechanisms of two-way coupling in particle-laden isotropic turbulence. *Phys. Fluids* **2003**, *15*, 315–329. [CrossRef]
17. Elghobashi, S. On predicting particle-laden turbulent flows. *Appl. Sci. Res.* **1994**, *52*, 309–329. [CrossRef]
18. Maxey, M. The gravitational settling of aerosol particles in homogeneous turbulence and random flow fields. *J. Fluid Mech.* **1987**, *174*, 441–465. [CrossRef]
19. Xiao, W.; Jin, T.; Luo, K.; Dai, Q.; Fan, J. Eulerian–Lagrangian direct numerical simulation of preferential accumulation of inertial particles in a compressible turbulent boundary layer. *J. Fluid Mech.* **2020**, *903*, A19. [CrossRef]
20. Reeks, M. On the dispersion of small particles suspended in an isotropic turbulent fluid. *J. Fluid Mech.* **1977**, *83*, 529–546. [CrossRef]
21. Squires, K.; Eaton, J. Measurements of particle dispersion obtained from direct numerical simulations of isotropic turbulence. *J. Fluid Mech.* **1991**, *226*, 1–35. [CrossRef]
22. Onishi, R.; Takahashi, K.; Komori, S. Influence of gravity on collisions of monodispersed droplets in homogeneous isotropic turbulence. *Phys. Fluids* **2009**, *21*, 125108. [CrossRef]
23. Chaisemartin, S.D. Modèles Eulériens et Simulation Numérique de la Dispersion Turbulente de Brouillards qui S'évaporent. Theses PhD, Ecole Centrale Paris, Gif-sur-Yvette, France, 2009.
24. Petersen, A.; Baker, L.; Coletti, F. Experimental study of inertial particles clustering and settling in homogeneous turbulence. *J. Fluid Mech.* **2019**, *864*, 925–970. [CrossRef]

25. Ireland, P.; Bragg, A.; Collins, L. The effect of Reynolds number on inertial particle dynamics in isotropic turbulence. Part 2. Simulations with gravitational effects. *J. Fluid Mech.* **2016**, *796*, 659–711. [CrossRef]
26. Berk, T.; Coletti, F. Dynamics of small heavy particles in homogeneous turbulence: A Lagrangian experimental study. *J. Fluid Mech.* **2021**, *917*, A47. [CrossRef]
27. Innocenti, A.; Jaccod, A.; Popinet, S.; Chibbaro, S. Direct numerical simulation of bubble-induced turbulence. *J. Fluid Mech.* **2021**, *918*, A23. [CrossRef]
28. Fréret, L.; Thomine, O.; Reveillon, J.; Chaisemartin, S.D.; Laurent, F.; Massot, M. On the role of preferential segregation in flame dynamics in polydisperse evaporating sprays. In *Proceeding of the 2010 Summer Program*; Center for Turbulence Research, Stanford University: Stanford, CA, USA, 2011; pp. 383–392.
29. Pope, S. *Turbulent Flows*; Cambridge University Press: Cambridge, UK, 2000. [CrossRef]
30. Reveillon, J.; Guichard, L.; Hauguel, R. Direct Numerical Simulation of Statistically Stationary One- and Two-Phase Turbulent Combustion: A Turbulent Injection Procedure. *Flow Turbul. Combust.* **2004**, *73*, 133–167. .:APPL.0000049273.27776.f5. [CrossRef]
31. Overholt, M.; Pope, S. A deterministic forcing scheme for direct numerical simulations of turbulence. *Comput. Fluids* **1998**, *27*, 11–28. . [CrossRef]
32. Reveillon, J.; Demoulin, F.X. Effects of the preferential segregation of droplets on evaporation and turbulent mixing. *J. Fluid Mech.* **2007**, *583*, 273–302. [CrossRef]
33. Sabot, M. Eulerian Modeling and Numerical Methods for the Description of Turbulent Polydisperse Sprays. Ph.D. Thesis , Université Paris-Saclay, Gif-sur-Yvette, France, 2016.
34. Mehrabadi, M.; Horwitz, J.; Subramaniam, S.; Mani, A. A direct comparison of particle-resolved and point-particle methods in decaying turbulence. *J. Fluid Mech.* **2018**, *850*, 336–369. [CrossRef]
35. Gai, G.; Thomine, O.; Hadjadj, A.; Kudriakov, S. Modeling of particle cloud dispersion in compressible gas flows with shock waves. *Phys. Fluids* **2020**, *32*, 023301. [CrossRef]
36. Woittiez, E.; Harm, J.; Portela, L. On the Combined Effects of Turbulence and Gravity on Droplet Collisions in Clouds: A Numerical Study. *J. Atmos. Sci.* **2009**, *66*, 1926–1943. [CrossRef]
37. Rouson, D.; Eaton, J. On the preferential concentration of solid particles in turbulent channel flow. *J. Fluid Mech.* **2001**, *428*, 149–169. [CrossRef]
38. Monchaux, R.; Bourgoin, M.; Cartellier, A. Analyzing preferential concentration and clustering of inertial particles in turbulence. *Int. J. Multiph. Flow* **2012**, *40*, 1–18. . [CrossRef]
39. Letournel, R.; Laurent, F.; Massot, M.; Vié, A. Modulation of homogeneous and isotropic turbulence by sub-Kolmogorov particles: Impact of particle field heterogeneity. *Int. J. Multiph. Flow* **2020**, *125*, 103233. . [CrossRef]
40. Hogan, R.; Cuzzi, J. Stokes and Reynolds number dependence of preferential particle concentration in simulated three-dimensional turbulence. *Phys. Fluids* **2001**, *13*, 2938–2945. [CrossRef]
41. Gai, G.; Hadjadj, A.; Kudriakov, S.; Mimouni, S.; Thomine, O. Numerical Study of Spray-Induced Turbulence Using Industrial Fire-Mitigation Nozzles. *Energies* **2021**, *14*, 1135. [CrossRef]